

Quantifying Changes in the Spatial Structure of Trabecular Bone

Norbert Marwan^{1,2,*}, Gise Beller³, Dieter Felsenberg³,
Peter Saparin^{4,†}, Jürgen Kurths^{1,5}

¹ Potsdam Institute for Climate Impact Research (PIK)
14412 Potsdam, Germany

² Interdisciplinary Center for Dynamics of Complex Systems, University of Potsdam
14415 Potsdam, Germany

³ Charité, Campus Benjamin Franklin, University of Medicine Berlin
12200 Berlin, Germany

⁴ Department of Biomaterials, Max Planck Institute of Colloids and Interfaces
14424 Potsdam-Golm, Germany

⁵ Department of Physics, Humboldt University Berlin
12489 Berlin, Germany

We apply recently introduced measures of complexity for the structural quantification of distal tibial bone. For the first time, we are able to investigate the temporal structural alteration of trabecular bone. Based on four patients, we show how bone may alter due to temporal immobilisation.

PACS: 05.45.-a, 07.05.Pj, 87.57.Nk, 87.59.Fm, 87.61.Pk

*email: marwan@pik-potsdam.de

†Presently with Perceptive Informatics, a PAREXEL technology company, Am Bahnhof Westend 15, 14059 Berlin, Germany

1. Introduction

The whole human body is a highly complex and dynamic system ensuring adaptation to a changing environment. Consequently, the human skeletal system is continuously changing in order to adapt its strength especially to current loading conditions. However, in subjects suffering on certain bone diseases, like osteoporosis (loss of bone mineral density and increased) fracture risk), limited moveability, or staying in micro-gravity conditions, bone may change so dramatic that the bone will lose a significant amount of its stability and fracture risk increases. These changes are on the one hand loss of bone mass, a decrease of the mineralisation of bone, and on the other hand a change in the micro-architecture of the interior bone (trabecular bone). Structural changes in trabecular bone have received much attention in the last years because the loss of bone mass alone cannot explain all variation in bone strength. Moreover, the rapid progress in high resolution Computed Tomography (CT) imaging facilitates the investigation of the micro-architecture of bone.

The standard method for the quality assessment of the micro-architecture of trabecular bone is histomorphometry [Parfitt *et al.*, 1983; Ito *et al.*, 1998; Hildebrand *et al.*, 1999]. More recent and advanced approaches quantify the complexity of trabecular structures by using measures of complexity based on symbolic dynamics [Saparin *et al.*, 1998, 2005], recurrence [Marwan *et al.*, 2007a], fractal [Marwan *et al.*, 2007b] or geometric properties [Marwan *et al.*, 2009], or using volumetric spatial decompositions [Stauber & Müller, 2006]. Applying these approaches on 3D images of trabecular bone, it was shown that the micro-architecture changes substantially during the development of osteoporosis. The main conclusions in [Saparin *et al.*, 2005; Marwan *et al.*, 2007b, 2009] were that the complexity of the bone micro-architecture decreases in the course of bone loss whereas the volume and surface of the trabecular structure changes in a different amount. This latter conclusion confirms former findings that the shapes of the trabeculae change during bone loss (e.g. from plate-like structure to rod-like structure) [Hildebrand *et al.*, 1999].

In this study we apply recently developed measures of complexity to characterise for the first time the temporal change of complex spatial structures of trabecular bone. We analyse the changes of the 3-dimensional micro-architecture of distal tibia of patients who suffered on temporal immobilisation due to a disease or an accident on the left body side. Moreover, we investigate the effects of errors in positioning of volume of interest within the bone during the follow-up CT scans and of choosing different segmentation parameters.

2. Data and Methods

For our analysis, we have used data from the *Advanced Detection of Bone Quality (ADOQ)* study. In this framework, different subject groups were investigated in order to develop reference data for high-resolution 3D peripheral Quantitative Computer Tomography (3D-pQCT). It includes 3D data from patients suffering from ligament rupture or fracture of the extremity, or from hemiplegic patients (half of the body is paralysed).

For each patient the 3D-pQCT investigations were performed over a period of six months including baseline imaging and four follow-up measurements with an interval of six weeks. The measurements were performed at all extremities: left and right distal radii and distal tibiae. In our investigation we focused on distal tibia. We have selected four patients, who have attended the follow-up measurements at least three times, and who had suffered temporal immobility due to a disease or an accident on the left body side.

The data were acquired in-vivo by XtremeCT 3D-pQCT scanner (Scanco Medical AG, Switzerland). The 3D-pQCT images have an isotropic voxel size of $82 \mu\text{m}$, the image matrix has a size of $1536 \text{ voxels} \times 1536 \text{ voxels} \times 110 \text{ voxels}$ (length of the imaged region along the bone axis was 9.02 mm ; Fig. 1). The clinical situation of the remaining patients is summarised in Tab. 1.

The pQCT images were converted from 3D-pQCT data format into a 3D mesh format for our analysis using the Amira software platform (Mercury Computer Systems Inc.).

The comparison of follow-up 3D-pQCT scans was done by considering the common regions overlapping in all scans (see also Subsect. 3.1). This was necessary because the scan at different time points causes slight displacements of the imaged regions of distal tibia. To minimise deviations due to dislocations/

Table 1. Diagnosis of the four patients whos tibial bone structure was imaged by 3D-pQCT and assessed by the structural measures of complexity.

| Patient ID | Clinical Diagnosis | Follow-up visits |
|------------|--|------------------|
| 5 | medial fracture on the left femoral neck | 5 |
| 9 | ligament rupture left knee | 4 |
| 11 | media infarct (stroke) with left-sided failure/ strong distal paralysis, caused wheel-chair dependence | 3 |
| 14 | impression fracture on the left tibial plateau | 4 |

displacements, the pQCT device establishes common regions for all of the scans. However, small tilts cannot be corrected with this method, hence leading to potential variations in structural analysis.

For the quantification of the bone microarchitecture we focus only on the trabecular part of the bone. Therefore, to separate the trabecular bone from the rest of the imaged 3D data we created manually volumes of interest (VOI). Then, in order to reduce the level of noise in the pQCT data, the 3D images were filtered using a 3D median filter. Bone and marrow voxels were separated by using of a global thresholding; the threshold level was set to 2800 units of the pQCT image (this value was found heuristically by looking at the histogram of the attenuation values, but also see Subsect. 3.2).

At first, we calculated the classical measure bone volume fraction BV/TV which provides information about the amount of bone material. Then we calculated recently introduced structural measures of complexity (SMCs), which are basing on symbol encoding, curvature, translational invariance and local shape of trabecular bone elements (Tab. 2) [Saparin *et al.*, 2005; Marwan *et al.*, 2005, 2007b, 2009].

SMCs based on symbol encoding use a limited set of structural elements or symbols for the quantification of the 3D structures. The purpose of the symbol-encoding procedure is to reduce the amount of information in a 3D-pQCT image to its essential structural composition by representing the bone architecture. The modified symbol-encoding procedure for the micro-CT data is based on an alphabet of three different symbols: M, marrow voxel; I, internal bone voxel; and S, surface bone voxel. Bone “surface” is a one voxel-thick layer of bone voxels which are lying at the boundary between two tissues: bone and marrow. Based on distributions and joint distributions of the symbols, the measures of complexity are defined. For example, the surface complexity index SurfCI is defined by

$$SurfCI = - \sum_{VOI} p_{surf} \log_2 p_{surf}, \quad (1)$$

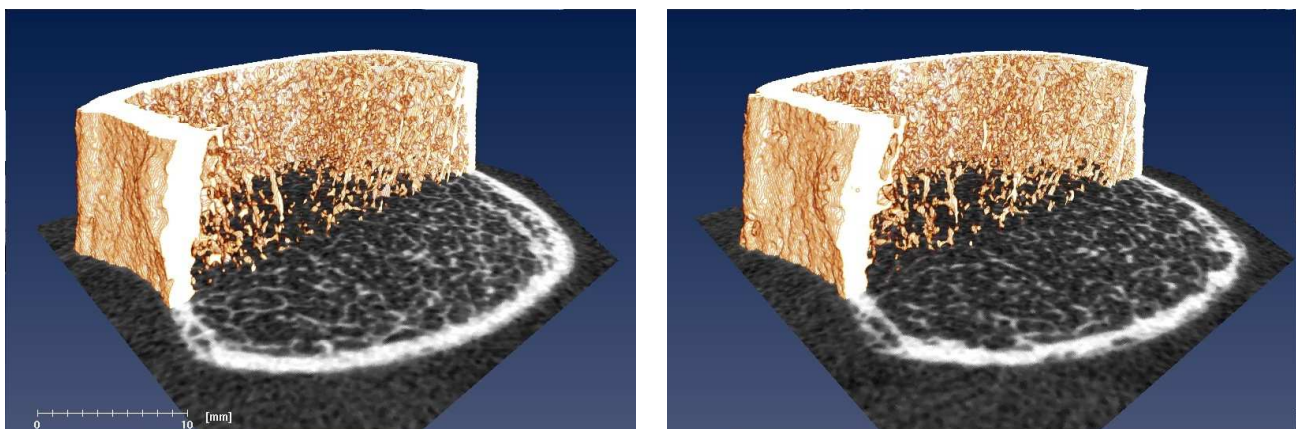


Fig. 1. 3D-pQCT images of left distal tibia of patient 9 at the beginning of the study (left panel) and after four months at the end of the study (right panel) showing slight variations of the bone micro-architecture. The lower, gray-scale plane represents a 2D orthoslice, and the coloured volume rendering shows a cutted part of the 3D image.

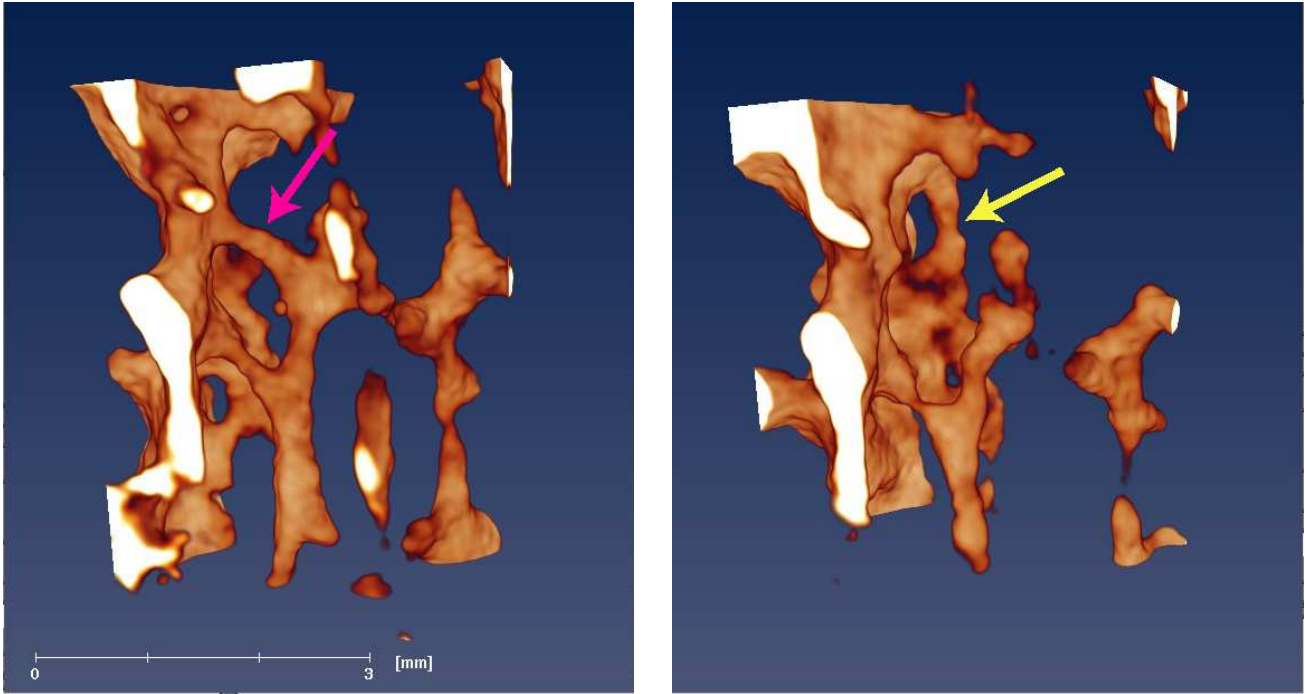


Fig. 2. A detail of the 3D-pQCT image shown in Fig. 1, at the beginning of the study (left panel) and after four months at the end of the study (right panel). The thinning and resorption of trabeculae is visible (magenta arrow). But new trabeculae can also appear (yellow arrow).

with p_{surf} as the distribution of local surface indices

$$p_{\text{surf}} = \frac{p_{\text{loc}}(S)}{p_{\text{loc}}(I) + p_{\text{loc}}(S)}. \quad (2)$$

This measure is calculated in a small moving box VOI. SurfCI assesses the complexity of the distribution of bone surface voxels in 3D. Other SMCs based on symbol encoding quantify the complexity or the distribution of the trabecular structures [Saparin *et al.*, 2005].

The main idea behind the SMCs basing on the geometrical shape is based on the fact that different 3D objects of the same volume have different surfaces, depending on their geometrical shape. For example, a long cylinder (length is much larger than radius) has a larger surface than a cube of the same volume,

Table 2. Structural measures of complexity (SMCs) used in this study.

| | | |
|--|---|-----------------------------|
| <i>SMCs based on symbol encoding</i> [Saparin <i>et al.</i> , 1998, 2005] | 3D Normalised Entropy of geometrical locations of bone tissue | S_n |
| | Structure Complexity Index, based on bone volume fraction | $\text{SCI}_{\text{BV/TV}}$ |
| | 3D Structure Complexity Index | SCI_{3D} |
| | Surface Complexity Index | SurfCI |
| | Surface Index of Global Ensemble | SurfIGE |
| <i>Measures based on local shape and curvatures</i> [Marwan <i>et al.</i> , 2005; ESA MAP team AO-99-030, 2005; Marwan <i>et al.</i> , 2009] | Shape Complexity | SHC |
| | Averaged Shape Index | ASHI |
| | Shape Mutual Information | MISH |
| | Marching Cubes Entropy Index | MCE |
| | Marching Cubes Complexity | MCC |
| | total curvature | K |
| mean curvature | H | |
| <i>Measures assessing translational invariance</i> [Marwan <i>et al.</i> , 2007b] | Lacunarity | Λ |
| | Morans's I index | I |

whereas a sphere has the smallest possible surface for the same given volume. Therefore, the ratio between volume and surface is used in the definition of several SMCs, like the the local shape index

$$\sigma_{\text{loc}} = \frac{S_{\text{bone}}}{S_{\text{sphere}}} \quad \text{with} \quad S_{\text{sphere}} = 6\sqrt[3]{\pi\hat{V}_{\text{bone}}^2}, \quad (3)$$

where S_{bone} is the surface of trabecular bone in a small box, V_{bone} is its volume, and S_{sphere} is the smallest possible surface for such volume (which corresponds to the surface of a sphere). The average of the local shape index ASHI, as well as the measures SHC and MISH, are able to distinguish between different shapes with the same volume but whose surface differ, like plates and rods. MCE and MCC quantify the complexity of the bone surface [Marwan *et al.*, 2009].

Further measures base on fractal properties, translational invariance and small-scale spatial auto-correlation. For example, the lacunarity Λ measures the variation of the bone fraction in small moving boxes by using the ratio of the second and first moment of the distribution $n(s, r)$ of the bone density:

$$\Lambda(r) = \frac{\mu_2(r)}{\mu_1^2(r)}, \quad (4)$$

where the first and second moments are

$$\mu_1(r) = \frac{1}{N} \sum_s s n(s, r) \quad \text{and} \quad \mu_2(r) = \frac{1}{N} \sum_s s^2 n(s, r), \quad (5)$$

N is the total number of boxes, s the local bone density and r is the size of the moving box [Marwan *et al.*, 2007b]. The lacunarity measures therefore how homogenously distributed the trabecular bone is.

As we have mentioned, several SMCs are basing on analysis of ensembles of local properties estimated from a moving cubic box. The size of the moving cubic box should be small enough to locally quantify structural elements, but large enough to cover a sufficient surface necessary to distinguish between different shapes and to reduce artefacts. Based on this requirements, we have found empirically a trade-off for the box size to be $20 \times 20 \times 20$ voxels ($1.64 \times 1.64 \times 1.64$ mm).

The SMCs have been calculated on the trabecular bone of the distal tibia within the specified VOI. As the same bone region was scanned at six weeks intervals, for the first time the results allow us to study structural changes in the same trabecular bone over time.

3. Experiments to test stability and reproducibility of the structural measures

Stability and reproducibility of the measures are crucial requirements to any data analysis tools. In the following we present our studies of the influence of main disturbing factors, including mismatch of VOIs and different bone segmentation thresholds. In another study we have investigated effects of the image resolution [Marwan *et al.*, 2009].

3.1. Local mismatch of VOI or common region

For the study of structural changes during time, the 3D-pQCT images of the distal tibia have to be acquired at exactly the same location in order to provide images of bone appropriate for longitudinal evaluation. Therefore, the software of the pQCT device calculates the common region between consecutive images. Nevertheless, small deviations in the positioning of the common region still remain, e.g. due to tilts. Therefore, we analysed the variation of the SMCs for an artificial dislocation of the VOI.

In this numerical experiment we used 3D-pQCT data of the left distal tibia from patient with ID 9. We reduced the original VOI by removing a small $82 \mu\text{m}$ thick volume at its perimeter (that was defined as 1 voxel from each side in the xy -plane) and applied small random local displacements of the VOI in the xy -plane in the interval of ± 0.95 voxels (corresponding x - and y -shifts were randomly uniformly distributed between -77 and $77 \mu\text{m}$). The calculations were repeated 500 times in order to get distributions of the measures from randomly displaced volume of interest. (Tab. 3).

Due to the random shifts by maximal of one voxel, the variation range of the SMCs was between 0.65% (S_n) and 37.0% (H). As a variation range we consider here the distance between the 5%- and 95%-quantiles

Table 3. Median and variation range of the structural measures of complexity for small random local displacements of VOI in interval from $\pm 77 \mu\text{m}$ (corresponding approximately to less than one voxel). The results are obtained from 500 realisations of random displacements of the VOI in CT images of distal tibia of patient ID 9.

| Measure | Median | Std. Deviation | $q_{0.05}$ | $q_{0.95}$ | Range (%) |
|----------------------|--------|----------------|------------|------------|-----------|
| BV/TV | 0.22 | 0.01 | 0.20 | 0.23 | 13.14 |
| SCI _{3D} | 0.76 | 0.01 | 0.73 | 0.77 | 4.39 |
| SCI _{BV/TV} | 0.90 | 0.01 | 0.89 | 0.91 | 2.37 |
| SurfCI | 0.86 | 0.01 | 0.84 | 0.86 | 2.22 |
| SurfIGE | 0.70 | 0.03 | 0.69 | 0.75 | 9.39 |
| S_n | 0.93 | 0.00 | 0.93 | 0.93 | 0.65 |
| H | 1.03 | 0.15 | 0.91 | 1.29 | 37.01 |
| K | -1.88 | 0.10 | -2.08 | -1.75 | 17.59 |
| Moran's I | 0.75 | 0.01 | 0.73 | 0.75 | 3.23 |
| Λ | 0.41 | 0.03 | 0.35 | 0.43 | 19.36 |
| ASHI | 1.73 | 0.01 | 1.73 | 1.76 | 1.70 |
| MISH | 0.19 | 0.00 | 0.19 | 0.19 | 1.14 |
| SHC | 0.22 | 0.00 | 0.22 | 0.23 | 2.99 |
| MCC | 5.72 | 0.03 | 5.67 | 5.75 | 1.28 |
| MCE | 0.65 | 0.01 | 0.64 | 0.67 | 4.83 |

normalised by the median value of the measure. Therefore, this performance measure allows us to assess the influence of the local displacement on the SMCs. We find that the measures BV/TV, the curvatures H and K as well as Λ are rather sensitive to the displacement with variation ranges above 10%. In contrast, the measures SCI_{BV/TV}, SurfCI, S_n , ASHI, MISH, SHC and MCC are much less sensitive, below 3%. The remaining measures, SCI_{3D}, SurfIGE, Moran's I and MCE are slightly more sensitive with the variation range around 5%.

These are crucial findings, because they imply that we cannot interpret as significant relative variations in the range below 5% (that is a half of the maximal range of 10% found in our simulations) in such measures as BV/TV and SurfIGE, and even variations around 10–20% in the curvatures H , K as well as Λ , as reflection of real structural changes, just because it is impossible to exclude positioning errors due to the minor shifts of the VOI during consecutive CT measurements. In the interpretations of the results derived from the ADOQ data in Sect. 4 we will take into account these error ranges.

Next, we compared the SMCs calculated from the entire 3D-pQCT images and the measures obtained from the common regions that match in different time-points. After evaluating the structure in the common regions, we have repeated the calculations of the SMCs for left distal tibia of patients with ID 5 and 9 for the entire trabecular VOIs that are larger than the common regions of the same measurements. The differences in results derived from the common region and the entire trabecular VOI are rather small for most of the SMCs (Tab. 4). In general, the typical trend in the behaviour of the measures found in matched regions remains the same when the entire VOIs are analysed (Fig. 3). Remarkable differences in the changes in time occur in the measures SCI_{3D} (only patient 5), SurfIGE, MISH (only patient 5, see Fig. 4), MCE and Moran's I index. Large differences in the absolute values were found in MISH, H and K . However, for H and K the trend remains very similar when matching regions and entire trabecular VOI are compared.

3.2. Dependence on the segmentation threshold

The choice of the bone segmentation threshold is an important step for evaluation of bone architecture. Therefore, we have studied how the choice of segmentation threshold affects the different SMCs. For this experiment we have used the 3D-pQCT images from patient 5. The bone segmentation threshold was set to values of 2300, 2800, 3200 and 4000 according to a threshold value correspondingly set too low, optimal value, too high, and extremely high.

We found that absolute values of all SMCs depend on the segmentation thresholds. For some measures like SCI_{3D}, SCI_{BV/TV}, K and Λ , their absolute values for the extreme thresholds 2300 and 4000 differ much from the values of the thresholds 2800 and 3200 (Fig. 5). For several measures, as BV/TV, SCI_{3D},

Table 4. Maximal and mean relative differences between the structural measures calculated for common region and for entire vertebral VOI of the images of patients ID 5 and 9.

| Measure | Patient No. 5 | | Patient No. 9 | |
|----------------------|---------------|---------------|---------------|---------------|
| | max. dev. (%) | mean dev. (%) | max. dev. (%) | mean dev. (%) |
| BV/TV | 2.4 | 1.4 | 3.8 | 2.6 |
| SCI _{3D} | 1.5 | 0.9 | 0.9 | 0.6 |
| SCI _{BV/TV} | 0.5 | 0.3 | 0.6 | 0.4 |
| SurfCI | 1.1 | 0.7 | 1.0 | 0.6 |
| SurfIGE | 4.0 | 2.3 | 4.0 | 2.5 |
| S_n | 0.1 | 0.0 | 0.1 | 0.0 |
| H | 11.3 | 7.1 | 11.0 | 6.5 |
| K | 33.3 | 21.3 | 19.3 | 13.1 |
| Moran's I | 0.9 | 0.5 | 1.2 | 0.8 |
| Λ | 2.8 | 1.4 | 2.7 | 1.7 |
| ASHI | 1.1 | 0.7 | 0.4 | 0.3 |
| MISH | 21.8 | 16.9 | 0.4 | 0.3 |
| SHC | 6.3 | 4.6 | 0.8 | 0.6 |
| MCC | 0.8 | 0.5 | 0.3 | 0.2 |
| MCE | 2.3 | 1.4 | 2.1 | 1.4 |

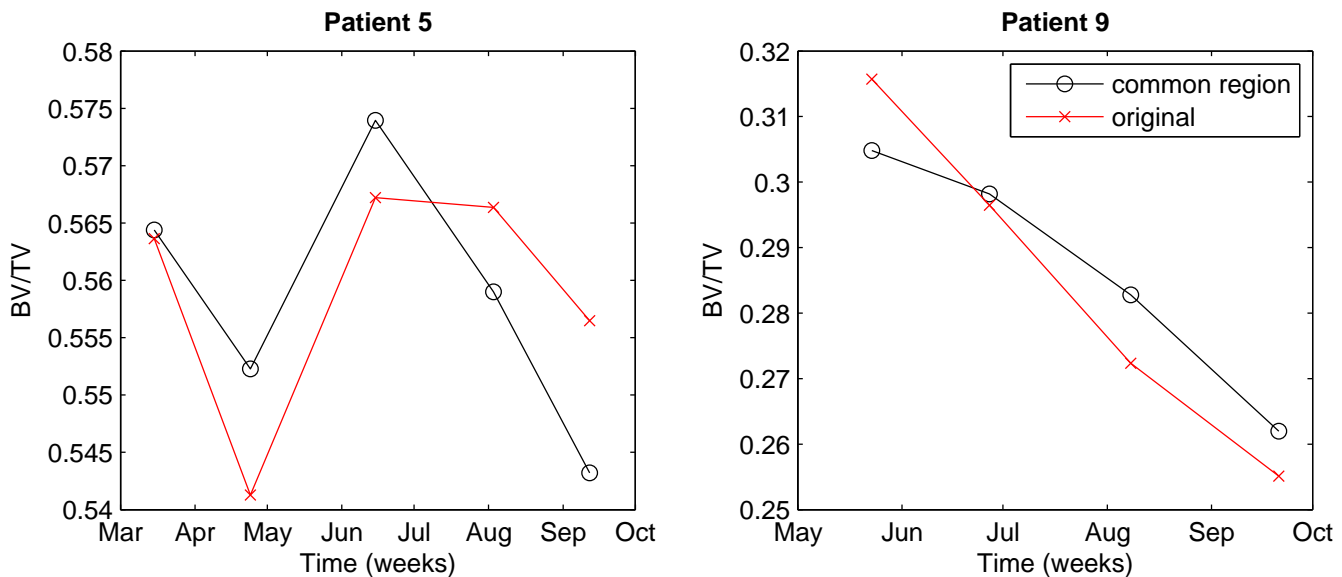


Fig. 3. The BV/TV calculated from the entire trabecular VOIs and the common regions of left distal tibiae for patients 5 and 9.

SCI_{BV/TV}, SurfCI, S_n , H , K , Λ , MISH and MCC we found a different trend only for the extreme low and extreme high threshold levels, whereas for levels of 2800 and 3200, the trend remained similar. Similar evolution in time were found for the other measures SurfIGE, Moran's I , ASHI, SHC and MCE indicating that the trend (or qualitative behaviour) of these measures is not as sensitive to the choice of the threshold as of the other measures (Fig. 6). Large differences for the longitudinal behaviour, and hence high sensitivity, were found for the measures H , K and MCC.

These results confirm that our choice of the bone segmentation threshold at the level of 2800 is appropriate, because more extreme threshold values like 2300 or 4000 reveal more different results (but in the same direction). Moreover, this numerical experiment demonstrates that a slight change of the threshold would not affect the qualitative findings how the SMCs evolve with time.

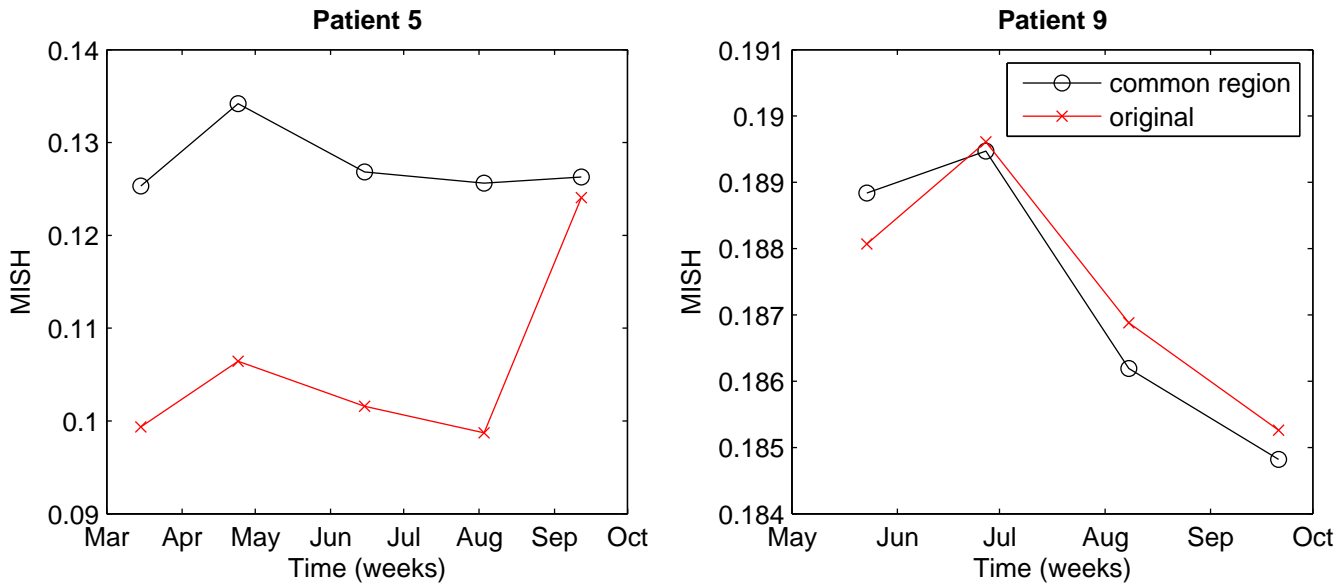


Fig. 4. The shape mutual information MISH calculated from the entire trabecular VOIs and the common regions of left distal tibiae for patients 5 and 9.

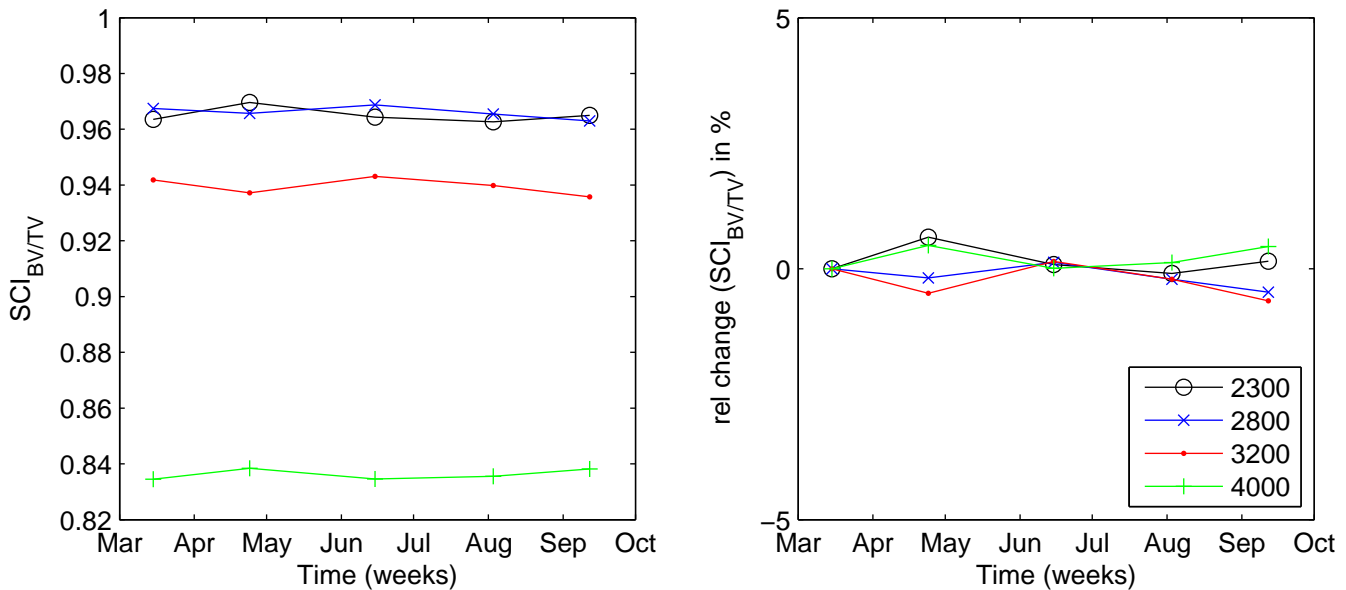


Fig. 5. Exemplary shown SMC for different values of bone segmentation threshold reveals large difference in the absolute values for the threshold level set extremely high (here 4000 pQCT units) or low (2300 pQCT units).

4. Evaluation of 3D-pQCT data from ADOQ Study

The set of 3D structural measures of complexity was applied to evaluate the architectural changes of trabecular bone in patients of temporal immobility, imaged by 3D-pQCT obtained during the ADOQ study. In order to compare SMCs with classical histomorphometry we use the trabecular thickness Tb.Th. The findings in regards of the stability and reproducibility of the structural measures reported in Section 3 were used to validate the range if changes of the SMCs have been found in longitudinal study (except the Tb.Th, because this measure was calculated directly by the pQCT device). The results of the evaluation are shown in Figs. 7–11.

Considering the BV/TV of all the four analysed patients and comparing the left and right distal tibiae,

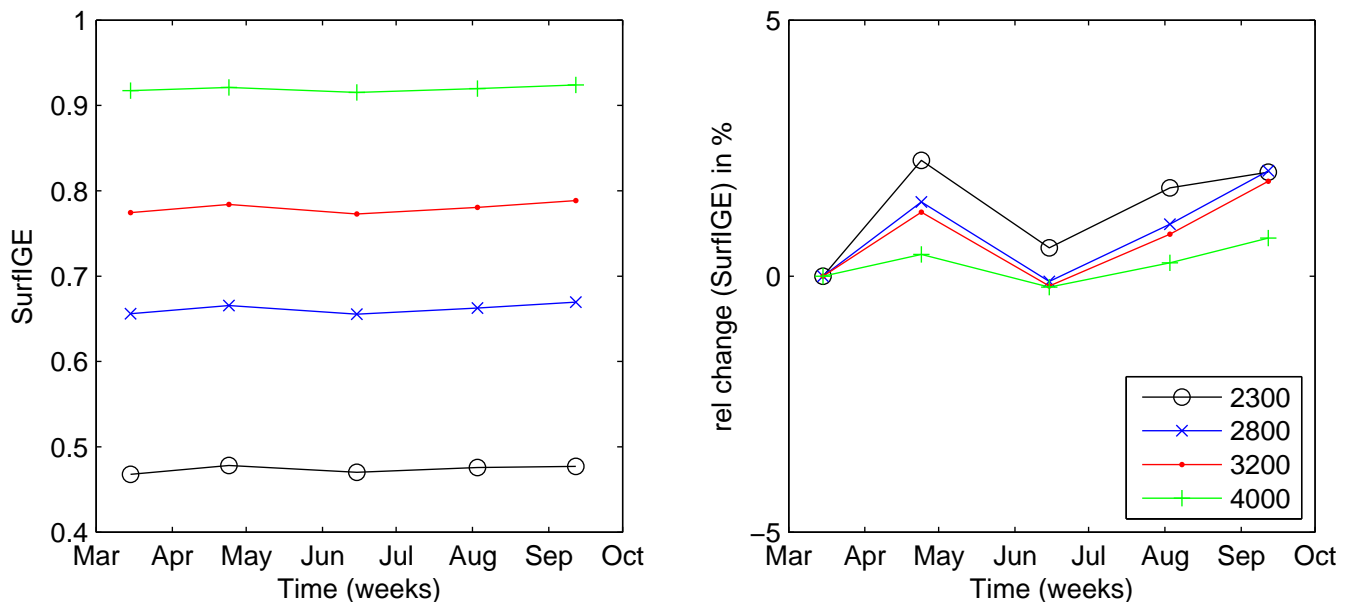


Fig. 6. Exemplary shown SMC for different values of bone segmentation threshold reveals different absolute values but same qualitative behaviour.

we observe bone degradation in patients 5 and 9, whereas the BV/TV for patients 11 and 14 remained almost constant (Fig. 7). This is especially surprising for patient 11, because after the stroke he was partly disabled and needed a wheel-chair. Most likely the rehabilitation therapy after the stroke was very effective. In contrast, patient 9 experienced a clear decrease in BV/TV, in particular on the left distal tibia, probably because the patient saved his left leg. The BV/TV of the patient 5 tibiae decreased slightly.

For **patient 11** (left-sided paralysis after stroke) we found that all measures did not change significantly during the investigated interval (see Figs. 7–11). Except for ASHI and MISH, whose range of change is rather small, all relative changes remained within the range of measurement-to-measurement variability due to positioning of the VOI. Moreover, from our analysis we can conclude that this patient (as well as patient 5) has probably the strongest bone among all considered patients: BV/TV of patients 11 and 5 has the highest values, its trabecular architecture is very complex, as it is indicated by high SCI_{3D} , the mean curvature H is lowest (and even negative), ASHI has lowest values suggesting more convex trabecular structure, what is typical for a dense trabecular bone. From the viewpoint of bone morphometry, the proximal tibiae of patient 11 are also characterised by the highest Tb.Th (Figs. 11).

Patient 14 (impression fracture left tibial plateau) has an intermediate level of bone volume fraction and complexity of trabecular bone structure (Figs. 7–11). For this patient most of the measures have their values between the extreme values of patients 9 and 11. However, during the investigated period of time, the trabecular bone has not changed much as it is indicated by the structural measures which vary only within their error range. We found a slight increase of the surface complexity of the affected left distal tibial trabecular bone after week 10, as revealed by the measures SurfCI, S_n , ASHI and SHC (all $< 1\%$). Moreover, the mean curvature H increased slightly, suggesting a small amount of thinning of the trabeculae.

The SMCs for **patient 5** (fracture on the left femoral neck) reveal that this patient has also strong bone, as observed by high bone density, high complexity of the trabecular architecture, and low values of the mean curvature H (that is also negative). During the investigation period, the trabecular bone composition is only slightly changing (Figs. 7–11). The bone density decreased up to -5% , the structural complexity as quantified by SCI_{3D} decreased only by -2% , and the variability of local trabecular shapes decreased (measured by an increase of ASHI by 2.5% , MISH by 15% , and a decrease of SHC by -7%). H varied during the investigated period, but finally increased (25%). The other measures vary only slightly or do not allow reliable interpretations because the range of variations is within the measurement-to-measurement error range. Nevertheless, it is remarkable that the left and right side seems to be affected in a similar

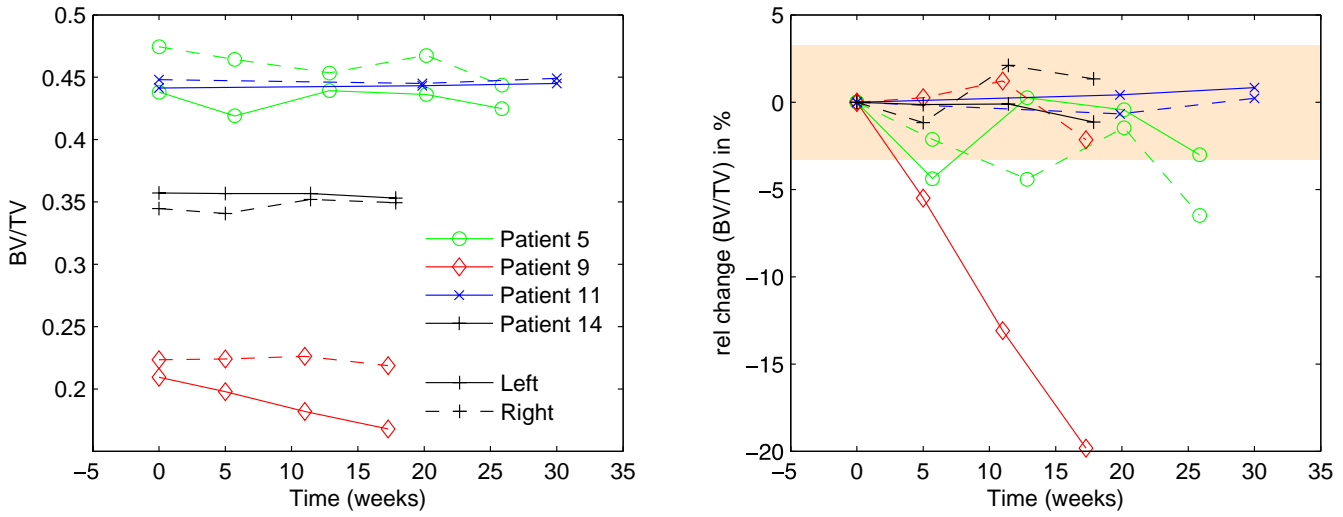


Fig. 7. Bone volume fraction BV/TV expressed in % (left panel) and its relative change (right panel) during the consecutive measurements after trauma or disease caused immobility of the left limb. The rose-shaded region marks the range of variation caused by positioning errors.

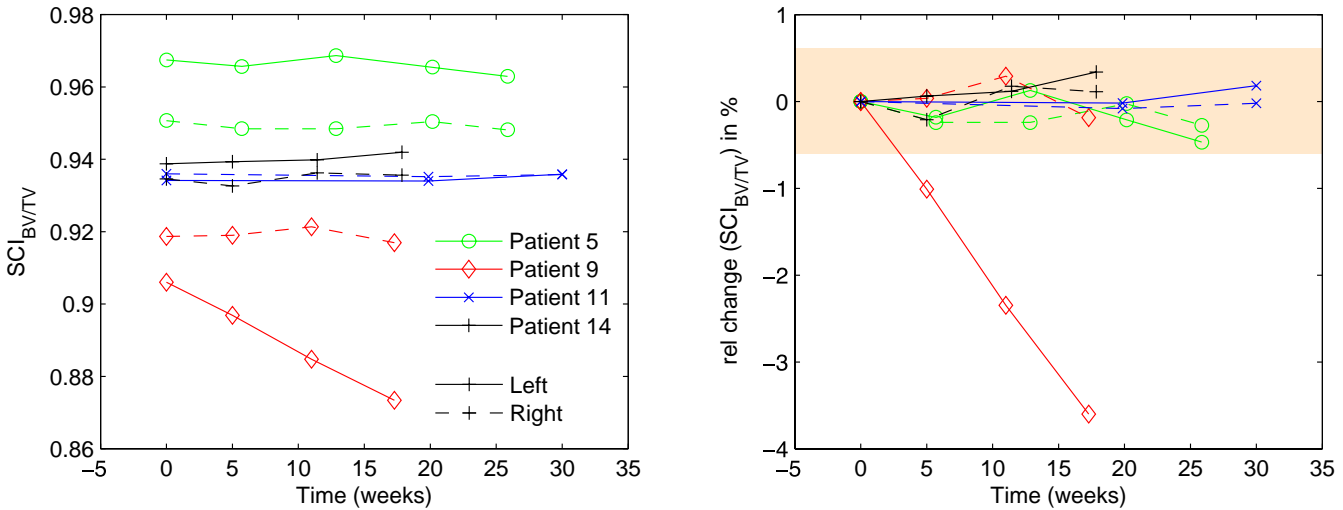


Fig. 8. Structural complexity measured by $SCI_{BV/TV}$ (left panel) and its relative change (right panel) during the consecutive measurements after trauma/ disease caused immobility of the left limb. The rose-shaded region marks the range of variation caused by positioning errors.

way; the structural measures vary on both sides with same amplitudes. However, for several measures we found anti-correlation between the values obtained from the left and the right side (e.g. in BV/TV , SCI_{3D} , total curvature K , $ASHI$ or MCE). This could be caused by an alternative loading of the left and the right sides (starting with the right because the left side suffered the fracture).

In contrast, **patient 9** (ligament rupture) turned out to be the patient with lowest bone density and lowest complexity of the trabecular microarchitecture. This patient experienced a dramatic degradation of trabecular bone as expressed by a decrease of bone volume fraction (up to -20%) and significant changes of the trabecular structure during the investigation period of 17 weeks, in particular on the left side (which was the affected side by the ligament rupture; see Figs. 7–11). The thinning of the trabeculae is well expressed by the increase of the mean curvature H (50%) and the decrease of $Tb.Th$ (-20%). The structural complexity as quantified by SCI_{3D} decreased by -7% (this change is also confirmed by the other SMCs like $SCI_{BV/TV}$, $SurfCI$, and $SurfIGE$). The degradation of the trabecular structure caused an

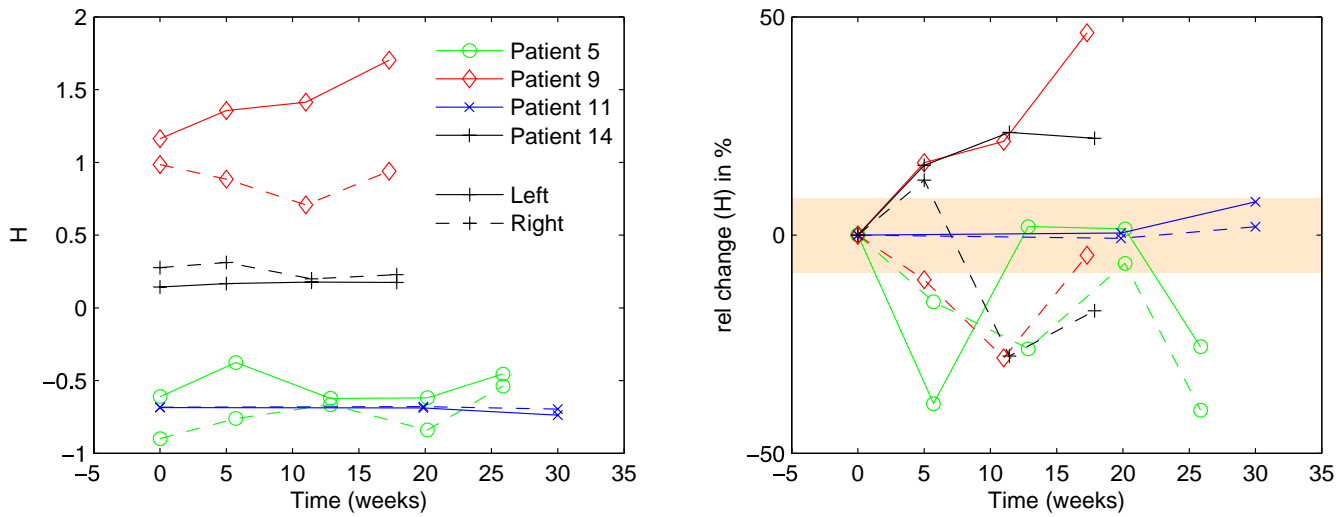


Fig. 9. Mean curvature H (in mm^{-1} , left panel) and its relative change (right panel) during the consecutive measurements after trauma/ disease caused immobility of the left limb. The rose-shaded region marks the range of variation caused by positioning errors.

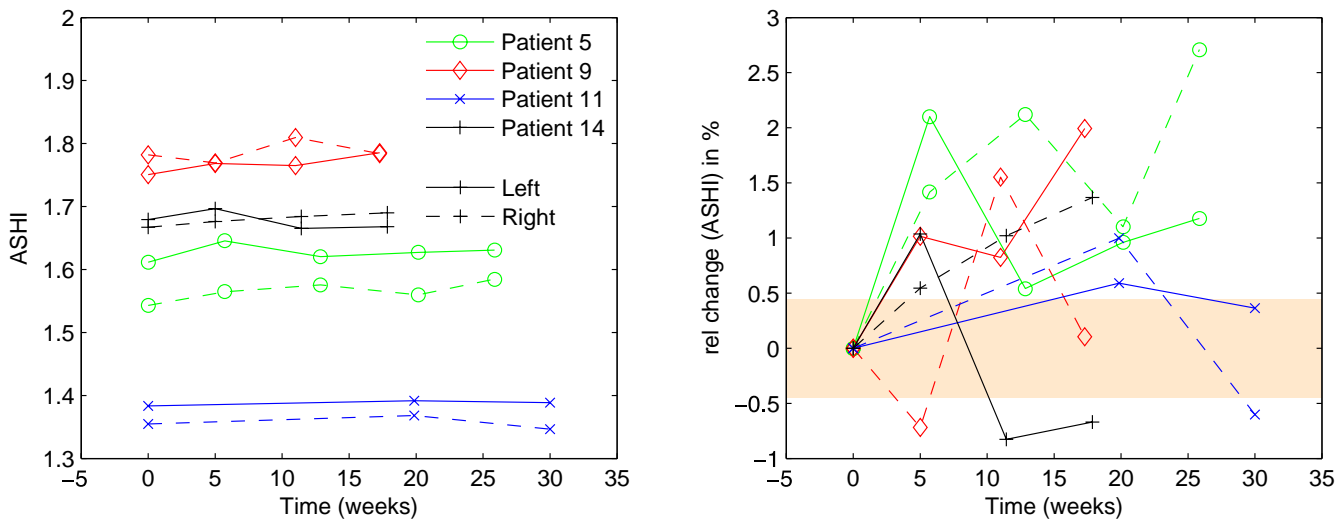


Fig. 10. Shape complexity measured by ASHI (left panel) and its relative change (right panel) during the consecutive measurements after trauma/ disease caused immobility of the left limb.

increase of the variability of the local shape of bone's structural elements, expressed by a decreasing of MISH by -4% .

5. Conclusions

We have applied recently introduced structural measures of complexity (SMC), which are based on symbol encoding, curvature, translational invariance and local shape of trabecular bone elements, to trabecular bone structure in distal tibia. For the first time, we have been able to study temporal alterations in 3D trabecular bone structure using SMCs.

The developed SMCs are able to detect and assess the temporal alterations in the trabecular bone structure in distal tibia due to temporal immobility. The detected structural variations have been different from subject to subject due to different disease or sites of the fractures, as well as different treatment. For two patients the range of change of some measures was smaller than their measurement-to-measurement variability range due to the errors in positioning of the imaged part of the tibia, suggesting a positive effect

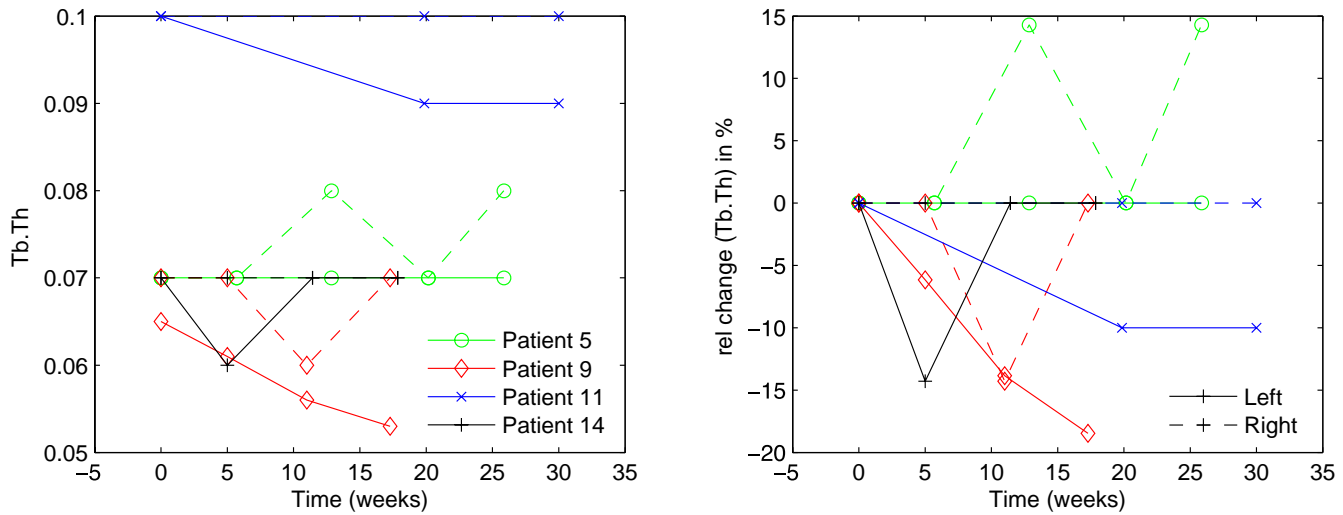


Fig. 11. Trabecular thickness Tb.Th (in mm, left panel) and its relative change (right panel) during the consecutive measurements after trauma/ disease caused immobility of the left limb.

of the preventive treatment. The developed SMCs based on the shape index are sensitive to structural changes; their range of change is significant and exceeds the interval of measurement-to-measurement variation due to different positioning of the analysed limb.

Moreover, we have investigated the effect of small displacements of the imaged volume during the pQCT scan and influence of different bone segmentation thresholds. Using simulations of artificial position errors of the volume of interest we have been able to define a 95% variation (confidence) level for the SMCs. In the future, the SMCs will be further systematically studied by applying models for bone remodelling (e.g. [Huiskes *et al.*, 2000; Weinkamer *et al.*, 2004; Rusconi *et al.*, 2008]).

Our findings support that the recently proposed SMCs are useful to investigate trabecular bone alterations [Saparin *et al.*, 2005; Marwan *et al.*, 2005, 2007b, 2009]. This study has demonstrated their abilities to quantify longitudinal changes. In particular they can be applied in clinical diagnosis or monitoring when 3D-pQCT imaging is available.

Acknowledgments

This study was co-funded by the Microgravity Application Program/ Biotechnology from the Human Spaceflight Program of the European Space Agency (project MAP AO-2004-125), by the European Commission ADOQ study (Contract QLK-CT-2002-02363, Key action No. 6) and the Swiss government, and received support from Siemens AG and Scanco Medical AG. We thank Hans-Christian Hege and Steffen Prohaska, Zuse Institute Berlin (ZIB), for the support and help with the Amira software, as well as Jesper Skovhus Thomsen, Peter Fratzel and Wolfgang Gowin for fruitful discussions.

References

- ESA MAP team AO-99-030 [2005] *Assessment of Bone Structure and its Changes in Microgravity*, in: *SP-1290 "Microgravity Applications Programme: Successful Teaming of Science and Industry"* (ESA publications division, ESTEC, Noordwijk), ISBN 92-9092-971-5, pp. 282–305.
- Hildebrand, T., Laib, A., Müller, R., Dequeker, J. & Rüeggsegger, P. [1999] "Direct Three-Dimensional Morphometric Analysis of Human Cancellous Bone: Microstructural Data from Spine, Femur, Iliac Crest, and Calcaneus," *Journal of Bone and Mineral Research* **14**, 1167–1174, doi:10.1359/jbmr.1999.14.7.1167.
- Huiskes, R., Ruimerman, R., van Lenthe, G. H. & Janssen, J. D. [2000] "Effects of mechanical forces on maintenance and adaptation of form in trabecular bone," *Nature* **405**, 704–707.

- Ito, M., Nakamura, T., Matsumoto, T., Tsurusaki, K. & Hayashi, K. [1998] “Analysis of trabecular microarchitecture of human iliac bone using microcomputed tomography in patients with hip arthrosis with or without vertebral fracture,” *Bone* **23**, 163–169, doi:10.1016/S8756-3282(98)00083-0.
- Marwan, N., Kurths, J. & Saparin, P. [2007a] “Generalised Recurrence Plot Analysis for Spatial Data,” *Physics Letters A* **360**, 545–551, doi:10.1016/j.physleta.2006.08.058.
- Marwan, N., Kurths, J., Thomsen, J. S., Felsenberg, D. & Saparin, P. [2009] “Three dimensional quantification of structures in trabecular bone using measures of complexity,” *Physical Review E* **79**, 021903, doi:10.1103/PhysRevE.79.021903.
- Marwan, N., Saparin, P. & Kurths, J. [2007b] “Measures of complexity for 3D image analysis of trabecular bone,” *The European Physical Journal – Special Topics* **143**, 109–116, doi:10.1140/epjst/e2007-00078-x.
- Marwan, N., Saparin, P., Thomsen, J. S. & Kurths, J. [2005] “An Innovative Approach for the Assessment of 3D Structures in Trabecular Bone,” *Journal of Gravitational Physiology* **12**, 127–128.
- Parfitt, A. M., Mathews, C. H. E., Villanueva, A. R., Kleerekoper, M., Frame, B. & Rao, D. S. [1983] “Relationships between Surface, Volume, and Thickness of Iliac Trabecular Bone in Aging and in Osteoporosis,” *Journal of Clinical Investigation* **72**, 1396–1409, doi:10.1172/JCI111096.
- Rusconi, M., Zaikin, A., Marwan, N. & Kurths, J. [2008] “Effect of Stochastic Resonance on Bone Loss in Osteopenic Conditions,” *Physical Review Letters* **100**, 128101, doi:10.1103/PhysRevLett.100.128101.
- Saparin, P. I., Gowin, W., Kurths, J. & Felsenberg, D. [1998] “Quantification of cancellous bone structure using symbolic dynamics and measures of complexity,” *Physical Review E* **58**, 6449, doi:10.1103/PhysRevE.58.6449.
- Saparin, P. I., Thomsen, J. S., Prohaska, S., Zaikin, A., Kurths, J., Hege, H.-C. & Gowin, W. [2005] “Quantification of spatial structure of human proximal tibial bone biopsies using 3D measures of complexity,” *Acta Astronautica* **56**, 820–830, doi:10.1016/j.actaastro.2005.01.007.
- Stauber, M. & Müller, R. [2006] “Age-related changes in trabecular bone microstructures: global and local morphometry,” *Osteoporosis International* **17**, 616–626, doi:10.1007/s00198-005-0025-6.
- Weinkamer, R., Hartmann, M. A., Brechet, Y. & Fratzl, P. [2004] “Stochastic Lattice Model for Bone Remodeling and Aging,” *Physical Review Letters* **93**, 228102, doi:10.1103/PhysRevLett.93.228102.

